Quaternary Science Reviews 97 (2014) 58–70

Contents lists available at ScienceDirect

Quaternary Science Reviews

journal homepage: www.elsevier.com/locate/quascirev

Abrupt variations of Indian and East Asian summer monsoons during the last deglacial stadial and interstadial

Bing Hong [a, *], Yetang Hong [a], Masao Uchida [b], Yasuyuki Shibata [b], Cheng Cai [a], Haijun Peng [a], Yongxuan Zhu [a], Yu Wang [a], Linggui Yuan [a]

[a] State Key Laboratory of Environmental Geochemistry, Institute of Geochemistry, Chinese Academy of Sciences, 46 Guanshui Road, Guiyang, Guizhou 550002, China
[b] Center for Environmental Measurement and Analysis, National Institute for Environmental Studies, Onogawa 16-2, Tsukuba, Ibaraki 305-0053, Japan

ARTICLE INFO

Article history:
Received 22 August 2013
Received in revised form
9 May 2014
Accepted 10 May 2014
Available online

Keywords:
Indian summer monsoon
East Asian summer monsoon
Westerly
ENSO
Last deglaciation
GHGs

ABSTRACT

The phase relationship between the Indian summer monsoon (ISM) and the East Asian summer monsoon (EASM) during the last deglaciation remains controversial. Here, we reconstruct a 15,000-year plant cellulose $\delta^{13}C$ proxy record for the ISM from the Yuexi peat bog in southwestern China. The record shows that the ISM abruptly decreases during the Younger Dryas (YD) stadial and abruptly increases during the Bølling–Allerød (BA) interstadial. A comparison of the Yuexi record with other related proxy climate records reveals two types of phenomena. First, the strengths of the two Asian monsoons are inversely related during the YD stadial, i.e., the ISM strength decreases and the EASM increases. During this period, the southern Chinese mainland consisted of a wide arid zone while the northern Chinese mainland was much wetter. The arid zone in southern China resulted from two different types of monsoon processes: the abnormal northward extension of the EASM rain belt, leading to less rainfall in southeast China, or an illusion that the EASM weakened. The other process is a real weakening of the ISM. Second, during the BA interstadial, the strengths of both the ISM and EASM clearly increased. However, the maximum strengths appear to have occurred in the Allerød period. During this period, the entire Chinese mainland, both northern and southern, experienced wet conditions. The abnormal climate pattern of wet in the north and dry in the south during the YD stadial occurs because of the combined effects of the strengthened EASM, intensified westerlies, and weakened ISM, which could be attributed to the response to the abrupt cooling in the high northern latitudes and to the El Niño-like activity in the equatorial Pacific. The widespread wet climate during the BA interstadial may be related to an abrupt increase in the greenhouse gases (GHGs) concentrations in the atmosphere and to the La Niña-like activity in the equatorial Pacific. These results contribute to a better understanding of the response of the Asian monsoon to global changes and present a geo-historical scenario for understanding the East Asian hydrological variations in the current global warming phase.

1. Introduction

Several abrupt millennial timescale temperature variations are prominent features of the climate during the last deglaciation. These variations have been clearly recorded in the $^{18}O/^{16}O$ ice core time series from the Greenland Ice Sheet Project 2 (GISP2) (Stuiver et al., 1995). Because these time series contain a widespread BA warming event and a widespread YD cooling event, the transition between the warm and cold climates during the period presents a unique opportunity to better understand the response of the Earth's climate system to external and internal forcings. The Asian summer monsoon system, which consists of the ISM and EASM, is an important component of the Earth's climate system. Understanding the response of the Asian monsoon system to the climate transition will contribute to a better understanding of the operation of the Earth's climate system. In addition, because more than three-fifths of the Earth's population depends on Asian monsoon rainfall for their food and livelihood, there is an urgent need to better understand and predict the hydrological variations in the current global warming environment. Therefore, understanding the behaviors of the Asian monsoons in the last deglaciation provides a valuable scenario from geological history.

* Corresponding author. Tel.: +86 851 5891248; fax: +86 851 5891609.
E-mail address: hongbing@vip.skleg.cn (B. Hong).

http://dx.doi.org/10.1016/j.quascirev.2014.05.006
0277-3791/

A recent review study (Tiwari et al., 2011) comparing marine and terrestrial paleoclimate records from South Asia suggests that the ISM fluctuated widely during the deglaciation, with weaker monsoons during colder episodes, such as the YD, and stronger monsoons during warmer episodes, such as the BA. However, this study does not cover the paleoclimate records from some east Asian regions that are influenced by the ISM, e.g., the Tibetan Plateau and its adjacent regions, and it does not include the activity of the EASM. Another study on global climate evolution during the last deglaciation briefly discusses the behaviors of the ISM and EASM during the transition period, mainly focusing on the results of a few stalagmite ^{18}O records from the southern Chinese mainland (Clark et al., 2012). To complement these studies, we present here a continuous peat cellulose $\delta^{13}C$ record of the ISM covering the past 15,000 years. By comparing this record with a variety of other monsoon proxy records, especially the EASM proxy records published in recent years, we attempt to clarify the abrupt variation, phase relationship, and possible forcing mechanisms of the two Asian monsoons during the last deglaciation.

2. Study region and methods

The researched peatland is located in Yuexi County in the Sichuan Province of southwestern China (Fig. 1). The peatland is near the southeastern edge of the Tibetan Plateau and is at the southern extent of the Hongyuan peat bog (site 24 in Fig. 1). The study site is a valley peat bog at an altitude of 1950 m above sea level. As previous studies have shown, the southeastern Tibetan Plateau, including the Hongyuan and Yuexi peatlands, is strongly influenced by the ISM (Hong et al., 2003; Wang et al., 2010). The annual average temperature is approximately 13 °C and the annual mean rainfall is approximately 1000 mm in the Yuexi region. Due to the influence of the monsoon, approximately 95% of the annual rainfall occurs in the period from May to September, with the primary rainfall season from June to August, consistent with the general precipitation rule of the ISM domain (Wang et al., 2003). Yunnan pine (*Pinus yunnanensis*) and evergreen sclerophyllous oaks (*Quercus senescens*, *Quercus rehderiana*, *Quercus gilliana*) dominate the vegetation around the peatland.

An approximately 6-m-long peat core (28°47′N, 102°57′E) was drilled using a Russian peat corer. The plant residues in the core sample are mainly composed of the vascular sedge family of C_3 plants, including *Carex* and *Kobresia*, which is similar to the plant composition of the Hongyuan peat profile located north of Yuexi (Hong et al., 2003). An improved sodium chlorite oxidation method was used to extract alpha-cellulose from the peat vegetation residues (Green, 1963; Hong et al., 2000). To determine the stable carbon isotopic composition in the cellulose, 2 mg of the cellulose samples was loaded into a borosilicate tube together with preheated copper (II) oxide. After drying in a vacuum, the tube was sealed with an oxy-gas torch and heated in a muffle furnace at 550 °C (Sofer, 1980; Hong et al., 2001). The resulting CO_2 gas was measured for stable carbon isotopes using a MAT-252 mass spectrometer. The stable carbon isotopes of the cellulose were expressed as $\delta^{13}C$ relative to the VPDB scale (Coplen, 1996); the overall precision was found to be better than ±0.1‰ (1σ).

Previous work has shown that the vascular sedge family of C_3 plants exhibits a sensitive physiological response to the relative humidity of the environment by regulating the opening and closing of leaf stomata. This activity leads to changes in the stable carbon isotopic composition of atmospheric CO_2 utilized in plant photosynthesis (Francey and Farquhar, 1982; Schleser, 1995). The variation of the herbaceous plant's $\delta^{13}C$ value reflects the variation of the environmental relative humidity or precipitation. Because both the

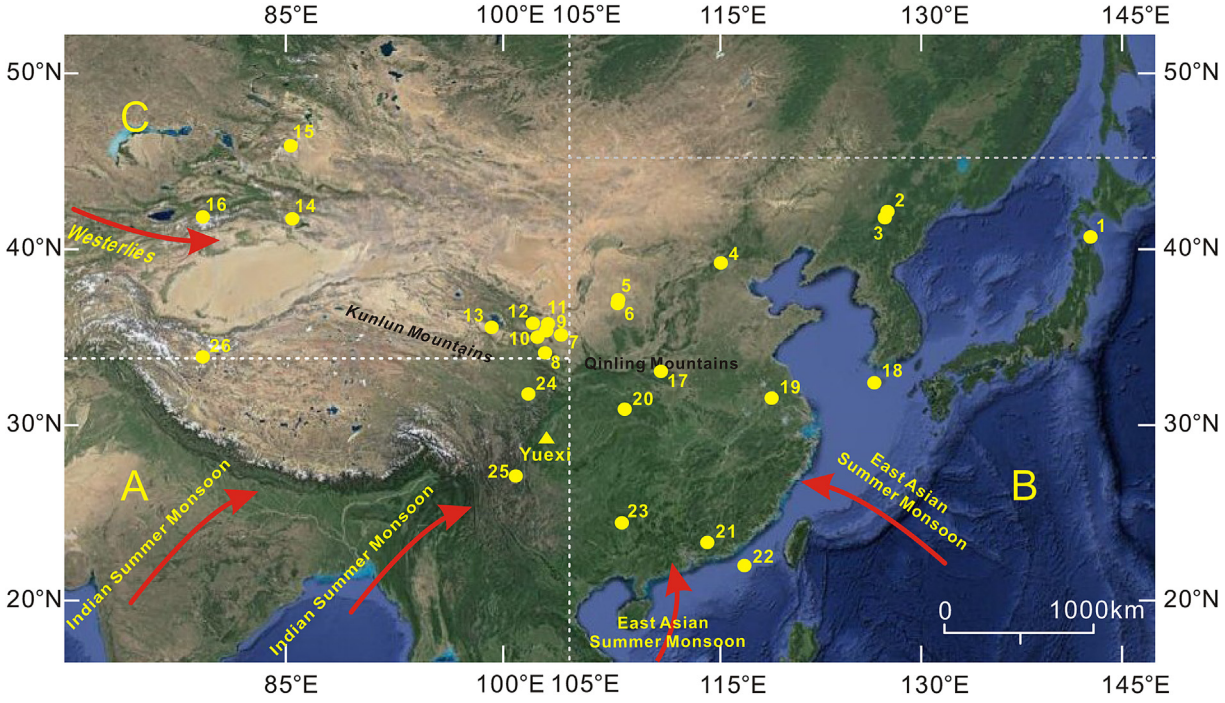

Fig. 1. Sketch map showing the location of the Yuexi peat bog (yellow triangle) and some of the related research sites (yellow circle). 1 — Tashiro, 2 — Sihailongwan, 3 — Hani, 4 — Kulishu, 5 — Jingbian, 6 — Midiwan, 7 — Lijiayuan, 8 — Dongxiang, 9 — Baxie, 10 — Yuanbao, 11 — Gaolanshan, 12 — Tuxiangtao, 13 — Qinghai Lake, 14 — Bosten Lake, 15 — Manas Lake, 16 — Yili, 17 — Dongshiya, 18 — Hanon, 19 — Hulu, 20 — Dajiuhu, 21 — Dahu, 22 — Core17940, 23 — Dongge, 24 — Hongyuan, 25 — Shayema, 26 — Sumxi Co. The three boxes define major summer precipitation areas: A — the Indian summer monsoon area, B — the East Asian summer monsoon area, and C — the westerly area (modified from Gao et al., 1962; Wang et al., 2003). The base map of Fig. 1 was obtained from the GoogleMaps by using screenshot software, and then the related research marks were added to the map by using the CorelDRAW Graphics Suite 12.

main growing season of herbaceous plants and the monsoon precipitation season are concurrent, i.e., from May to September, the variations of the $\delta^{13}C$ value for herbaceous plants reflect the changes of monsoon precipitation in the summer season. As a result, information on summer monsoonal rainfall changes at a given time can be preserved in the $\delta^{13}C$ values of peat plant cellulose. Finally, plant cellulose is highly resistant to decomposition. Both cellulose and its isotopes are highly stable over periods of approximately 10^5 years (Briggs et al., 2000). Recent advances in the extraction and purification of cellulose from batch-bulk peat samples have allowed application of the $\delta^{13}C$ value of peat cellulose to reconstruct the history of the Asian summer monsoon precipitation. The lower (or more negative) the $\delta^{13}C$ value in the peat cellulose is, the greater the rainfall, and vice versa. In addition, the evaluation of the summer monsoon intensity is still an issue discussed in the atmospheric physics community. Two potential definitions have been presented. One is based on the summer monsoon precipitation amount and the other is based on the wind regime of the summer monsoon (Huang et al., 2008). Some studies have suggested that both the wind and precipitation variations are good indicators of the intensity of the ISM and EASM (Wang et al., 2003). Here, we use the summer monsoon rainfall amount as an indicator of the Asian summer monsoon intensity, which has been widely accepted by the paleoclimate community (Chen et al., 2011; An et al., 2012). The greater the summer rainfall amount, the greater the summer monsoon intensity, and vice versa. Therefore, the lower (or more negative) the $\delta^{13}C$ value in the peat cellulose is, the greater the Asian summer monsoon intensity, and vice versa (Hong et al., 2001, 2003, 2005, 2010).

The core was divided into units of differing peat color and texture. Radiocarbon samples were used to bracket the changes in core sedimentology and then additional ages were used to further secure the chronology. Finally, 20 ^{14}C age control points were set up (Fig. 2; Table 1). The peat cellulose samples of the control points were prepared for graphite targets; their ^{14}C intensity was determined at the AMS Laboratory of the National Institute for Environmental Studies in Tsukuba, Japan, to obtain the ^{14}C age (Uchida et al., 2008). The chronological age was obtained after correction using the CALIB-4.3 program (Stuiver et al., 1998). We then obtained the calibrated ^{14}C age sequence of the Yuexi peat profile via linear interpolation. In the case of natural output the mean sedimentation rate in the entire Yuexi peat profile was approximately 36 cm per 1000 years, and the sedimentation rates at the interval from 14,598 to 12,681 cal yr BP exceeded 10 cm per 1000 years (Table 1), which is sufficient to resolve millennial-scale variability. The Yuexi peat core sample was cut continuously into 1-cm subsamples equivalent to a mean time resolution of approximately 27 years. The results of the upper 5.4 m portion of the Yuexi peat core (15,000 cal yr BP) are presented in this study.

We compare the data of Yuexi peat with several previously published paleoclimate records, most of which have been published in the last decade. These records have reliable chronologies and have presented information regarding the dry and humid conditions during the YD and/or BA periods.

3. Results and discussion

3.1. Abrupt variation of the ISM in the past 15,000 years

The southwest Chinese mainland is subject to the influence of the ISM. However, sensitive ISM proxy records spanning more than 15,000 years and covering the last deglaciation, such as the $\delta^{18}O$ record from the Dongge Cave stalagmite (Dykoski et al., 2005), are few. Although some paleolimnological sediments have a long history that covers the last glacial period, they do not record the abrupt variations and the transient nature of the ISM during the last deglaciation. It is thought that snow cover on the Tibetan Plateau may effectively buffer the impact of lower-magnitude events (Cook et al., 2011).

Our Yuexi peat cellulose $\delta^{13}C$ record presents new ISM information regarding two aspects. First, the record again confirms an important phenomenon in which the ISM precipitation shows a series of abrupt reductions on centennial to millennial timescales that correspond to the ice-rafted debris (IRD) cooling events numbered from 0 to 8 in the North Atlantic during the Holocene epoch (Fig. 3) (Fleitmann et al., 2003; Gupta et al., 2003; Hong et al., 2003). This teleconnection relationship is further expanded to the last deglaciation. Fig. 3 shows that from approximately 12,900 cal yr BP onwards, the $\delta^{13}C$ values of the Yuexi peat cellulose abruptly increase, indicating an abrupt decrease in ISM rainfall or a weakened monsoon. The weakening reaches a minimum around 12,500 cal yr BP. In the subsequent period of approximately 400 years, the ISM strength generally maintains a weak state, although there are some fluctuations in strength. From approximately 12,100 cal yr BP, the $\delta^{13}C$ values of the Yuexi peat cellulose begin to abruptly decrease, indicating a rapid increase in ISM rainfall or an increase in the monsoon's strength. The strengthening reaches a maximum around 11,800 cal yr BP. Taking the ^{14}C dating errors into

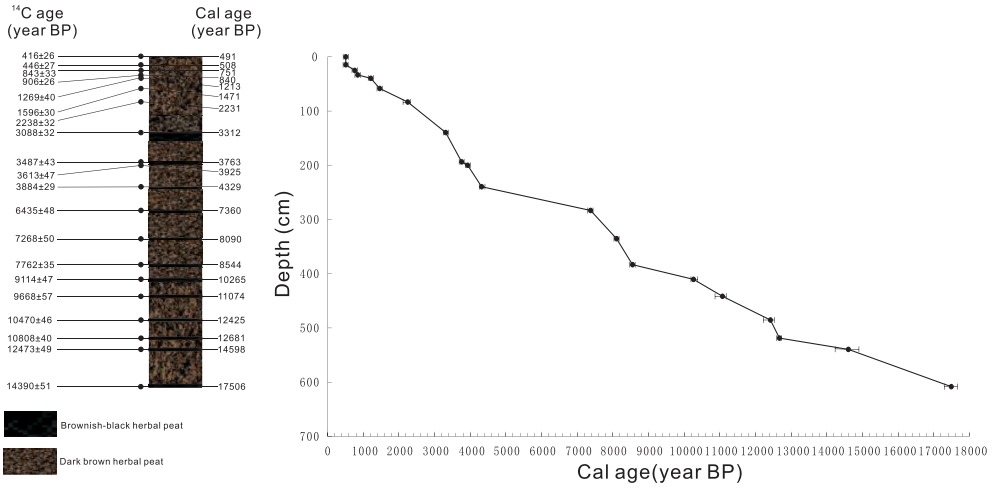

Fig. 2. Chronology and lithology of fresh peat core from the Yuexi peat bog. Black error bars show ^{14}C dates with 1σ error of the Yuexi peat profile.

Table 1
Radiocarbon dates of Yuexi peat profile.

Lab code	Sample ID	Depth (cm)	$\delta^{13}C$ (‰, VPDB)	^{14}C age (yr BP)	Calibrated age range (yr BP)	Calibrated age (yr BP)
TERRA-120310a25	YXI01	1	24.53	416 ± 26	477–509	491
TERRA-120310a16	YXI02	14	−24.95	446 ± 27	497–518	508
TERRA-121610a12	YXI03	24	−24.38	843 ± 33	700–787	751
TERRA-120310a23	YXI04	33	−25.24	906 ± 26	782–904	840
TERRA-113010b14	YXI05	40	−26.40	1269 ± 40	1176–1267	1213
TERRA-120310a14	YXI06	59	−26.18	1596 ± 30	1417–1528	1471
TERRA-120310a26	YXI07	84	−26.09	2238 ± 32	2162–2329	2231
TERRA-120310a29	YXI08	140	−26.28	3088 ± 32	3265–3361	3312
TERRA-113010b15	YXI09	193	−26.47	3487 ± 43	3703–3828	3763
TERRA-113010b16	YXI10	201	−25.74	3613 ± 47	3860–3980	3925
TERRA-120310a17	YXI11	240	−26.07	3884 ± 29	4259–4407	4329
TERRA-113010b17	YXI12	283	−26.01	6435 ± 48	7323–7419	7360
TERRA-113010b18	YXI13	335	−24.70	7268 ± 50	8021–8160	8090
TERRA-120310a27	YXI14	383	−25.07	7762 ± 35	8481–8591	8544
TERRA-113010b19	YXI15	411	−25.03	9114 ± 47	10,220–10,370	10,265
TERRA-113010b20	YXI16	442	−25.58	9668 ± 57	10,874–11,194	11,074
TERRA-113010b21	YXI17	485	−24.58	10,470 ± 46	12,226–12,543	12,425
TERRA-113010b22	YXI18	518	−24.88	10,808 ± 40	12,614–12,729	12,681
TERRA-120310a15	YXI19	539	−25.25	12,473 ± 49	14,243–14,887	14,598
TERRA-120310a20	YXI20	608	−24.59	14,390 ± 51	17,247–17,660	17,506

account, the decrease in ISM rainfall or the weakening of the monsoon's strength from approximately 12,900 to 11,800 cal yr BP inferred from the $\delta^{13}C$ values of the Yuexi peat should correspond to the YD cooling event that occurred from 12,900 to 11,700 cal yr BP in the North Atlantic region (Stuiver et al., 1995). This result coincides with the results from Dongge Cave and South Asia (Dykoski et al., 2005; Tiwari et al., 2011). Fig. 3 also demonstrates that corresponding to the Older Dryas (OD) (around 15,000 to 14,700 cal yr BP) and the Intra-Allerød cold periods (13,250–13,070 cal yr BP) (Stuiver et al., 1995), the ISM strength appears to confirm the weakening trend. However these results remain to be examined further because they require a better ^{14}C age constraint.

Second, the Yuexi peat record also shows variations in the strength of the ISM during the last deglacial interstadial. In the interval from approximately 14,700 to 13,300 cal yr BP, the $\delta^{13}C$ value decreases, indicating an increase in ISM rainfall or an intensification of the monsoon's strength (Fig. 3). It is generally thought that this time interval corresponds to the BA warm period in the $^{18}O/^{16}O$ ice core record of GISP2 (Stuiver et al., 1995). The strengthening ISM during the BA warm period has also been recorded in both the Dongge Cave stalagmite ^{18}O in East Asia and several proxy indicators in South Asia (Dykoski et al., 2005; Tiwari et al., 2011). It is worth noting, however, that the Yuexi peat record shows clear fluctuations in monsoon precipitation during the BA interstadial (Fig. 3). A significant increase in the ISM strength and amplitude appears to occur only from 14,000 to 13,250 cal yr BP, possibly corresponding to the Allerød warm period in the North Atlantic (Stuiver et al., 1995).

3.2. Hydrological variations in East Asia during the YD stadial

Based on the seasonal fields of the modern monsoon stream function, air pressure, humidity, and precipitation, the Chinese mainland and its adjacent areas have been divided into several different monsoon climate regions. It is climatologically thought that the 105° longitude line, which runs along the eastern flank of the Tibetan Plateau and through the Indo-China 'land-bridge', roughly delineates the ISM and EASM regions (Gao et al., 1962; Wang et al., 2003, 2008; Hong et al., 2010). For this study, the three boxes in Fig. 1 are applied to define major summer precipitation areas, i.e., the ISM region (5–34°N, 65–105°E), the EASM region (10–45°N, 105–145°E), and the westerly region (34–50°N, 65–105°E). Obviously, the classification of research sites near the line is more ambiguous. For instance, the Dongge Cave (site 23 in Fig. 1) is situated in the eastern side of the line, but its climate signal

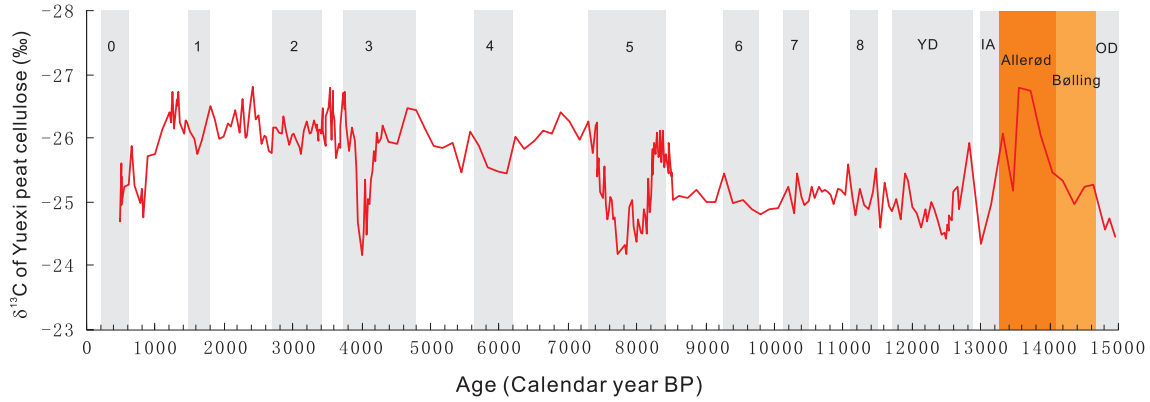

Fig. 3. The $\delta^{13}C$ precipitation proxy record of Yuexi peat cellulose for the Indian summer monsoon. Numbers from 1 to 8 indicate the eight North Atlantic ice-rafted debris (IRD) events (Bond et al., 1997). Number 0 indicates the 'Little Ice Age' event (Bond et al., 1997). The Younger Dryas, Inter-Allerod, and Oldest Dryas cooling events are denoted by YD, IA, and OD, respectively. The vertical gray bands trace the comparisons of precipitation anomalies for the Indian summer monsoon inferred from the Yuexi $\delta^{13}C$ with the cooling events. The vertical light red and red bands trace the comparisons of the precipitation anomalies of the monsoon with the Bølling and Allerød warming events.

has often been considered as representative of the ISM (Dykoski et al., 2005).

A previous study revealed a series of abrupt inverse phase variations between the ISM and EASM on centennial to millennial timescales that show the teleconnection relationship with the IRD cooling events in the North Atlantic Ocean during the Holocene (Hong et al., 2005). The inverse phase oscillation for the YD period has also been previously discussed (Hong et al., 2010). Our Yuexi peat record presents further evidence for the inverse phase variations. Fig. 4h shows the maximum $\delta^{13}C$ value of the Yuexi peat cellulose during the period from approximately 12,900 to 11,800 cal yr BP, indicating a decrease in ISM rainfall or a weakening of the monsoon's strength. As already discussed, this observation corresponds to the YD cooling event that occurred approximately between 12,900 and 11,700 cal yr BP in the North Atlantic (Stuiver et al., 1995) and also coincides with the results of Sumxi Co (site 26 in Fig. 1) (Gasse et al., 1991), Lake Shayema (site 25 in Fig. 1) (Jarvis, 1993), and the Dongge Cave (site 23 in Fig. 1) (Dykoski et al., 2005) in the ISM region of southwestern China and with other ISM records from South Asia (Tiwari et al., 2011).

However, the climate situation of the EASM region in the YD period is more complex. In general, it seems there is a climate-boundary situated roughly from the Kunlun Mountains to the Qinling Mountains on the Chinese mainland (at approximately 34°N) (Fig. 1). The vast area north of the boundary, including the northern EASM and westerly regions, has a wetter climate, while the southern EASM region has a drier climate or less rainfall. For example, the $\delta^{13}C$ value of the Tashiro peat cellulose in northeastern Japan clearly decreases (site 1 in Fig. 1), indicating an increase in EASM rainfall during the YD (also see Fig. 4a) (Shinozaki et al., 2011). In the Hani peatland of the northeastern Chinese mainland (site 3 in Fig. 1), located in the west of the Tashiro

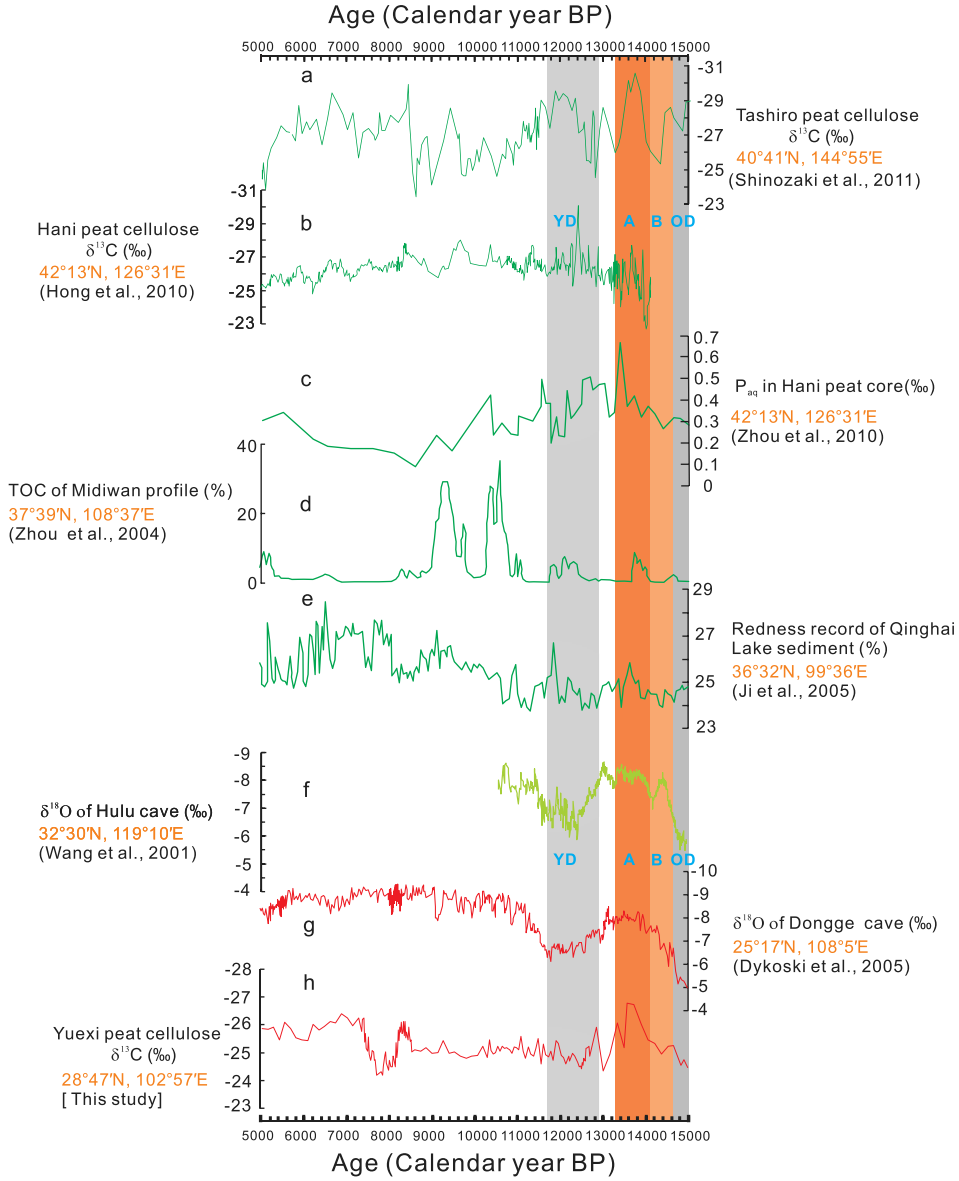

Fig. 4. Correlation of climatic events between the two Asian monsoons during the last deglaciation. The dark green color shows the precipitation proxy records of the East Asian summer monsoon in the region north of approximately 34°N. The light green color shows the precipitation records of the East Asian summer monsoon in the region south of approximately 34°N. The red color indicates the precipitation proxy records of the Indian summer monsoon. The Younger Dryas and Oldest Dryas cooling events are denoted by YD and OD, respectively. The Allerød and Bølling warming events are indicated by A and B, respectively. The vertical gray bands trace the comparisons of the precipitation anomalies of the two monsoons during the cooling periods. The vertical red and light red bands trace the comparisons of the precipitation anomalies during the warming periods.

peatland, a variety of proxy climate indicators, including peat cellulose $\delta^{13}C$ (also see Fig. 4b) (Hong et al., 2010), hydrogen isotope compositions ($\Delta\delta D$) (Seki et al., 2009), and *n*-alkane P_{aq} values of individual plant wax hydrocarbons (also see Fig. 4c) (Zhou et al., 2010), all record an especially moist local climate or more monsoonal precipitation during the period. In Lake Sihailongwan near the Hani peatland (site 2 in Fig. 1), the accumulation rates for biogenic silica (F-bSiO_2) exhibit several abnormal increases in the maxima during the YD (Schettler et al., 2006), the pollen percentage of *Larix*, *Picea*, and *Abies* reach their maximum (Stebich et al., 2009), and in particular, the thickness of the sediment varve of Lake Sihailongwan drastically oscillates with maximum peaks of up to 2 cm (Stebich et al., 2009). These phenomena have attracted a discussion about the local climate conditions of Sihailongwan (Hong et al., 2010). Considering the more monsoonal precipitation in the Hani district near Lake Sihailongwan during the YD, we cannot exclude the interpretation that the aforementioned phenomena of Lake Sihailongwan may also reflect a moist local climate or more monsoon precipitation (Hong et al., 2011).

The wetter climate signal during the YD period is also recorded in the sediment of the Loess Plateau in north-central China. The Baxie loess section (site 9 in Fig. 1) is located in the southeastern Loess Plateau where the rapid deposition of dust under cool, dry glacial conditions gave way to a period of soil development and reduced dust influx attributed to a strengthening of the moist summer monsoon during the YD (An et al., 1993). Furthermore, the Midiwan profile (site 6 in Fig. 1) is located in the central Loess Plateau of northeastern Baxie. A variety of proxy climate indicators in the profile, including tree and herb pollen concentrations, organic carbon content, and $\delta^{13}C$ values of organic carbon, all show different degrees of increased monsoon rainfall during the YD (Fig. 4d) (Zhou et al., 1996, 2004). The Jingbian and Dongxiang profiles provide additional evidence for a wetter climate in the YD. The Jingbian profile (site 5 in Fig. 1), which is near the Midiwan profile, has a YD sequence consisting of lacustrine silts, overlain by grayish black, silty peat and is dated from 12,730 to 11,850 cal yr BP. Zhou et al. demonstrated that both tree and herb pollen counts show a significant increase within the peat layer, signifying an increase in precipitation during the YD (Zhou et al., 2001). The Dongxiang profile (site 8 in Fig. 1) is located to the southwest of Midiwan and has a pedogenic paleosol layer, dated from 12,730 to 11,850 cal yr BP, indicating a more humid phase during the YD (Zhou et al., 2001). The Kulishu Cave (site 4 in Fig. 1) located to the northeast of the Midiwan provides a speleothem oxygen isotope record for the YD event in northern China (Ma et al., 2012). One of the most prominent features is that the Kulishu record clearly shows the three negative $\delta^{18}O$ excursions during the YD period centered at 12,410, 12,100, and 11,930 yr BP (^{230}Th dates and layer counting), indicating a clear increase in the monsoon rainfall.

In recent years, black carbon mass sedimentation rates (BCMSR) originating from regional paleofires have been used to assess the millennial scale wet–dry changes in the Loess Plateau region. The results of the Lijiayuan profile (site 7 in Fig. 1) reveal that "during the YD Chronozone, the background BCMSR shows three phases: a phase of relatively low background BCMSR bracketed by two phases of high background BCMSR. This indicates that a strong fire regime existed during the early and late stages of the YD Chronozone while a weak fire regime occurred in the middle stage (Page 67 of Wang et al., 2012a)." According to Fig. 4 presented by Wang et al., the so-called early and late stages of the YD Chronozone refer to two points in time around 12,500 and 11,200 cal yr BP, respectively, and the so-called middle stage refers to the more than 1300-year interval between the two time points. Because most of the weak fire regime from around 12,500 to 11,200 cal yr BP falls within the period of the YD event (around 12,900 to 11,700 cal yr BP; Stuiver et al., 1995), these results may imply a wetter climate of the Loess Plateau during the YD, although the wetter conditions do not necessarily mean reduced fire and vice versa. Additionally, in the western Loess Plateau, three thick loess profiles [i.e., Yuanbao, Gaolanshan, and Tuxiangtao (sites 10, 11, 12 in Fig. 1)] have been chosen to study rapid climatic changes (Chen et al., 1997). The results show high values of magnetic susceptibility and a low content of $CaCO_3$during the YD period (Fig. 4 of Chen et al., 1997), indicating more pedogenesis and hence summer precipitation.

Qinghai Lake (site 13 in Fig. 1), located west of Loess Plateau, is the largest closed-drainage saline lake in northwestern China. As early as the 1980s, a pioneering study noted that the lake water freshened and the lake level rose, possibly indicating the local wet climate during the YD (Kelts et al., 1989). This research indicated that "if this wet Qinghai episode is linked to the European record then the current model of a regionally-limited, Younger Dryas impact may require revision (Page 180 of Kelts et al., 1989)." Unfortunately, this idea did not attract enough attention, though this seemingly unusual phenomenon was later consistently confirmed. For example, this wet signal is also clearly recorded in a redness series in the sediment that originated from iron oxides near red beds or loess deposits transported fluvially into the lake (Fig. 4e) (Ji et al., 2005). Farther west in northern China, there is the largest inland freshwater lake called Bosten Lake (site 14 in Fig. 1), located in northern Xinjiang Province. Based on the lacustrine carbonate isotopic composition, sporopollen, and $CaCO_3$ analysis, the climate during the YD period was cold and relatively humid (Zhong, 1998). A wetter climate during the YD has also been tentatively proposed based on the investigation of Manas Lake (site 15 in Fig. 1), located in the northwest region of Bosten Lake (Rhodes et al., 1996).

In contrast, southeastern China and the adjacent area south of approximately 34°N generally had low rainfall during the YD. For instance, the Dongshiya Cave (33°47′N, 111°34′E) (site 17 in Fig. 1), southwest of the city of Luanchuan, Henan Province, is located on the southern slope of the Qinling Mountains. Therefore, a dry episode during the YD inferred from its stalagmite $\delta^{18}O$ record (Cai et al., 2008) provides strong evidence for a different climate on the two sides of the climate-boundary. Similar evidence can be found in the Hanon paleo-maar in Jeju Island, Korea (site 18 in Fig. 1), located at approximately the same latitude (33°15′N, 126°33′E) as the Dongshiya Cave. The very low content of total organic carbon in the maar sediment during the YD period indicates a local arid climate (Lee et al., 2008). Toward the south, the percentage of evergreen tree pollen in the Dajiuhu peatland (site 20 in Fig. 1) gradually decreases, indicating a decrease in the summer rainfall amount (Zhu et al., 2009). This finding coincides with the $\delta^{18}O$ results of the Hulu Cave stalagmite (site 19 in Fig. 1) (Fig. 4f) (Wang et al., 2001). At the same time, in the Dahu peatland (site 21 in Fig. 1), southeast of the Dajiuhu peatland, a decreasing TOC, relatively more positive $\delta^{13}C$ values, and a low accumulation of organic matter all indicate a dry climate (Zhou et al., 2004; Zhong et al., 2010). In the South China Sea (SCS), the diatom abundance of brackish-littoral species, e.g., *Cyclotelle* spp. and *Diploneis* spp., in the No. 17940 core sediment (site 22 in Fig. 1) was clearly distinguished, indicating an increase in salinity in the SCS. This increase has been attributed to the decrease in summer precipitation in South China that resulted in less freshwater passing through the Pearl River and into the SCS (Huang et al., 2009). In addition, the heavier $\delta^{18}O$ values of seawater in the MD01-2393 core from the mouth of the Mekong River at the southern extent of the SCS also suggest low rainfall during the YD period (Colin et al., 2010).

In summary, during the YD, there was a wetter region from northern Japan Island, through the Loess Plateau, and westward to the Xinjiang area of the northern Chinese mainland. At the same time, there was a drier region in southeastern China. Because the

climate of the ISM region west of 105° longitude was also drier during the YD, a widespread region from southeastern China and adjacent areas, through the Tibetan Plateau, and westward toward South Asia experienced a drier climate during that period (Fig. 5).

3.3. Hydrological variations in the Chinese mainland during the BA interstadial

As mentioned before, during the BA warm period, the records of Yuexi, Dongge (Fig. 4h and g), and South Asia (Tiwari et al., 2011) all suggest a humid climate or strengthening of the ISM. Unexpectedly, the EASM region, including both the northern and the southern EASM regions, also appears to have had a wetter climate, indicating a strengthening of the EASM (Fig. 6). For example, the diatom abundance of brackish-littoral species in the No. 17940 core sediment in the SCS indicated a relatively low level of seawater salinity, which suggested high EASM precipitation (Huang et al., 2009). Toward the north, in the Dahu peatland, an increase in the TOC, relatively more negative $\delta^{13}C$ values, and a higher accumulation of organic matter all indicate a wetter climate (Zhong et al., 2010). The humid climate has also been reflected in the stalagmite $\delta^{18}O$ record of the Hulu Cave (Wang et al., 2001). The maar sediment of Jeju Island, Korea, near the boundary line, suggests a cold and arid climate during the YD. However, during the BA, the sediment's multi-proxy data indicate warm and humid conditions (Lee et al., 2008). Toward the northern EASM area and adjacent regions, numerous proxy climate records, e.g., the Tashiro peatland (Shinozaki et al., 2011), Lake Sihailongwan (Schettler et al., 2006; Stebich et al., 2009), the Hani peatland (Seki et al., 2009; Hong et al., 2010; Zhou et al., 2010), the Baxie loess (An et al., 1993), the Midiwan profile (Zhou et al., 2004), and Qinghai Lake (Ji et al., 2005), all clearly indicate a humid climate.

The Yili Valley (site 16 in Fig. 1), located in the westernmost region of Xinjing Province, is dominated by westerly winds throughout the year because of the topography that is open to the west which allows westerly airflow. A palynology study of the Yili Valley has also revealed the relatively warm and humid climate during the BA period (Li et al., 2011), though the climate during the YD period is drier, which may be representative of climate change during those periods in the westerly area. Moreover, research in the Yili Valley has clearly shown climate fluctuations during the BA period. The largest peak of the *Artemisia*/Chenopodiaceae (A/C) ratio occurred in the Allerød period (Fig. 6 of Li et al., 2011), which implies a maximum in effective moisture or precipitation at that time. A similar phenomenon is also found in the Asian monsoon area. A variety of indicators in Fig. 4 also suggest that during this approximately 1420-year BA warm period, both the ISM and EASM rainfall or the strengths of the two monsoons are unstable and have fluctuating variations. However, their maximum strengths appear to occur in the Allerød period.

3.4. Dynamic mechanism for wet conditions in the north and dry in the south during the YD stadial

Recent studies suggest that the superposition of two factors, namely the variations of GHGs and the Atlantic meridional overturning circulation (AMOC), explain much of the variability in regional and global temperatures during the last deglaciation (Shakun and Carlson, 2010; Clark et al., 2012). However, the dynamic mechanism for the abnormal climate pattern with wet in the north and dry in the south in East Asia during the same period remains unclear. Several factors have been used to identify the dynamic processes.

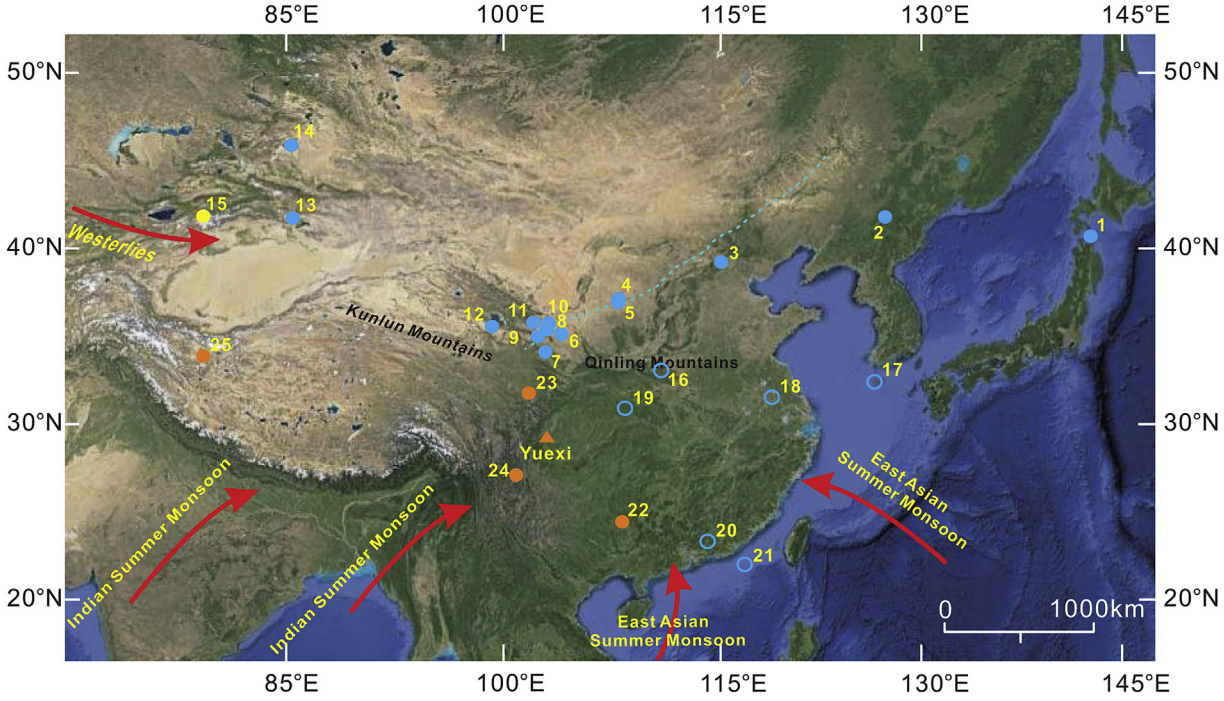

Fig. 5. Sketch map showing the abnormal climate pattern of the Chinese mainland and adjacent areas during the Younger Dryas stadial. The solid red circle and triangle denote the sites with dry climate conditions influenced by the Indian summer monsoon. A solid yellow circle denotes the site with dry climate conditions influenced by the westerlies. The solid blue circle and blue circle denote the sites with wet climate conditions influenced by the East Asian summer monsoon. 1 – Tashiro, 2 – Hani, 3 – Kulishu, 4 – Jingbian, 5 – Midiwan, 6 – Lijiayuan, 7 – Dongxiang, 8 – Baxie, 9 – Yuanbao, 10 – Gaolanshan, 11 – Tuxiangtao, 12 – Qinghai Lake, 13 – Bosten Lake, 14 – Manas Lake, 15 – Yili, 16 – Dongshiya, 17 – Hanon, 18 – Hulu, 19 – Dajiuhu, 20 – Dahu, 21 – Core17940, 22 – Dongge, 23 – Hongyuan, 24 – Shayema, 25 – Sumxi Co. The dashed line denotes the present-day limit of the summer monsoon (after Gao et al., 1962). The base map of Fig. 5 was obtained from the GoogleMaps by the same methods as Fig. 1.

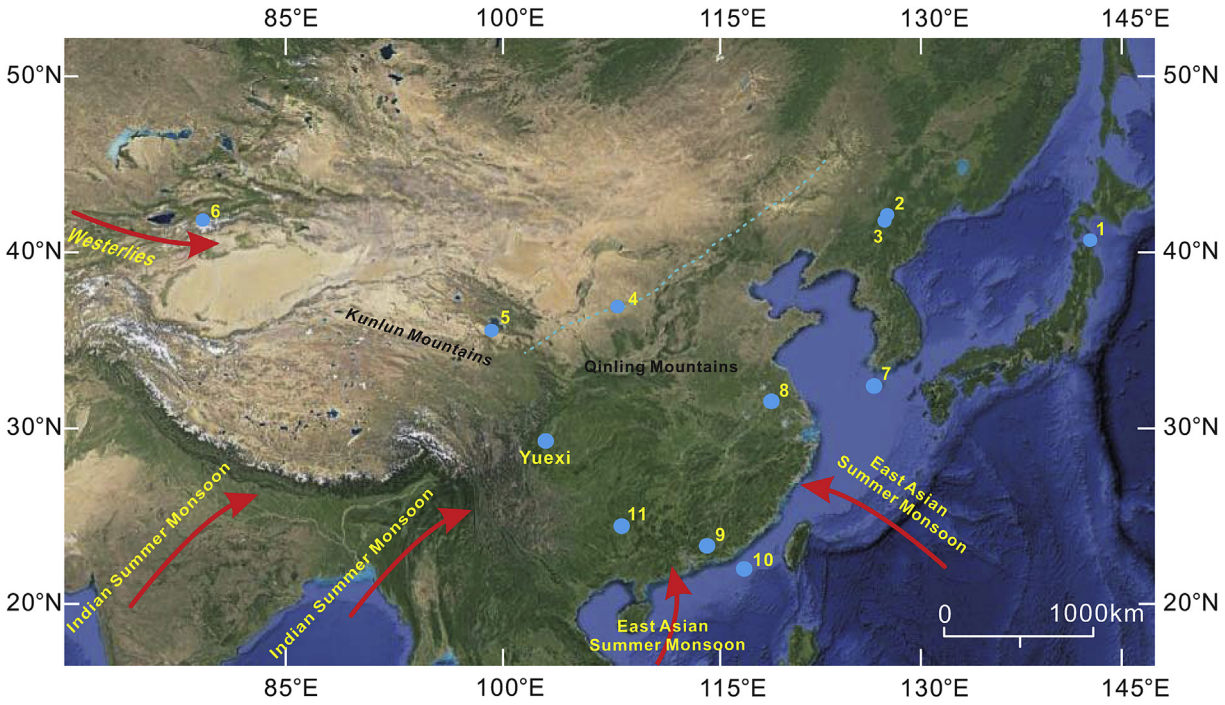

Fig. 6. Sketch map showing the wet climate pattern of the Chinese mainland and adjacent areas during the Bølling–Allerød interstadial. The solid blue circles denote the sites with wet climate conditions influenced by the Indian summer monsoon, the East Asian summer monsoon, and the westerlies. 1 – Tashiro, 2 – Sihailongwan, 3 – Hani, 4 – Midiwan, 5 – Qinghai Lake, 6 – Yili, 7 – Hanon, 8 – Hulu, 9 – Dahu, 10 – Core 17940, 11 – Dongge. The dashed line denotes the present-day limit of the summer monsoon (after Gao et al., 1962). The base map of Fig. 6 was obtained from the GoogleMaps by the same methods as Fig. 1.

3.4.1. Possible impact of ITCZ on precipitation variation

Shifts in the mean latitude of the Intertropical Convergence Zone (ITCZ) are generally accompanied by significant changes in hydrological quantities in the tropics and subtropics. The dry climate in the Asian monsoon region during the early and middle Holocene is generally thought to be evidence of a southward migration of the ITCZ (Wang et al., 2005; Fleitmann et al., 2007; Wanner et al., 2011), although records of aeolian sands and palaeosols from the northern margins of the EASM regions show a wetter early and middle Holocene (Yang et al., 2013). A southward shift of the ITCZ has also been used to explain the variability of monsoon precipitation during the last glacial period (Wang et al., 2001, 2006). However, the phase relationship of the Asian monsoons may provide a more complete constraint for the hypothesis. The impact of ITCZ migration would be correct if only the variation of the precipitation in the ISM region is considered. However, it is difficult to explain why increasing EASM rainfall occurs in northern Asia or why the EASM strengthens after the southward shift of the ITCZ. It is clear that there are other forcing factors in addition to the migration of the ITCZ.

3.4.2. Possible impact of cooling air temperature on effective moisture

A cooling climate may act to inhibit evaporation and thus to increase the effective moisture. Therefore, decreasing air temperature during the YD should be considered as one of the factors leading to wetter conditions in northern China. However, this does not appear to be the primary reason for the climate difference with wet conditions in the north and dry in the south because the climates of both northern and southern China cooled during the cooling episodes, e.g., the YD event. Moreover, in recent years, the actual evaporation conditions in the arid and semi-arid areas of northern China have been re-estimated by applying newer standardized techniques to hydrological simulations and data from field observations. The results show that the loss of water in these areas was not as significant as previously believed and that the moisture variability in these areas was dominated by variations of monsoon intensity and precipitation (Yang et al., 2011).

3.4.3. Effects of the westerlies

The westerlies are usually considered to affect northwest China in the middle latitudes. Specifically, the local summer rainfall may mainly result from transport of moisture by the westerly wind. As research progresses, understanding the climate dynamics of the westerly area has gradually deepened. A competitive relation between the growth and decline of the westerlies and the Asian monsoon has been gradually stressed. Currently, the focus of debate surrounds which factor is the dominant factor for the climate variation of northwest China, the westerly or the EASM. Some researchers have suggested, based on the study of vegetation and palynology, that the northern boundary of the Asian monsoon has moved in geological history and that the monsoon region covered the entire northern Chinese mainland, including northwestern China, during the last deglaciation and early-mid Holocene (Fig. 103 (d) of Winkler and Wang, 1993; Fig. 1 of Morrill et al., 2003). Considering the high water level of most lakes in northern and central Mongolia during the mid Holocene, some scientists have also speculated that the moisture-bearing summer monsoon may extend its influence westward to Xinjiang and northward to northern Mongolia (Rhodes et al., 1996; Tarasov et al., 2000, 2007; Blyakharchuk et al., 2007; Rudaya et al., 2009; Yang et al., 2011). In contrast, others have shown that on the orbital timescale, the arid central Asia region that is dominated by westerlies experienced synchronous and coherent moisture changes during the Holocene and that the effective moisture history in central Asia is out of phase with that in monsoonal Asia (Chen et al., 2008). This result implies that the monsoon barely extended to central Asia during the Holocene (Chen et al., 2008; Liu et al., 2008; Li et al., 2011). A recent

study used the flux of the >25-μm fraction in the Lake Qinghai sediment as a westerlies climate index (WI), with large WI values indicating strengthened westerlies and intensified aridification (An et al., 2012). The WI record shows that during the YD period, the WI value was large, reflecting intensified westerlies and resultant cold-dry impacts. This result clearly shows that the intensified westerlies did not transport more water vapor to northern China during the YD and therefore does not seem to be the primary reason for the widespread humid climate in northern China during that period.

In fact, in addition to the consideration of the water vapor amount, further verification of the effect of the westerlies from a kinetic perspective is more important. Based on the global reanalysis data sets provided by NCEP/NCAR, it is generally thought that in the background climate (or normal climatological conditions), the summer water vapor over the Chinese mainland originates mainly from the ISM and EASM transport. The water vapor transported by the mid-latitude westerlies is relatively weaker. In addition, the water vapor from westerlies mainly occurs in the higher atmosphere (500 hPa and above), while the monsoon moisture that greatly affects precipitation is mainly concentrated in the lower atmosphere (800 hPa and below) (Zhou and Yu, 2005; Wang and Chen, 2012). However, these findings do not mean that the effect of the westerlies can be neglected. The importance of the westerly, as a cold and dry airflow, is demonstrated when it encounters warm and humid monsoon water vapor that eventually results in the strong convergence over the main rainbelts, providing a highly beneficial background for abundant rainfall (Zhou and Yu, 2005). These results highlights that intensified westerlies and a strengthened EASM are the two indispensable factors during the YD. Their encounter and convergence in the atmosphere play a fundamental role in the occurrence of a humid climate in northern China during the YD.

3.4.4. Possible impact of the EAWN

In addition to the EASM, the impact of the East Asian winter monsoon (EAWM) on the regionally dry and wet condition may also need to be considered, since the precipitation inferred from some proxy climate indicators refers to the average precipitation for the whole year. Previous studies have revealed that in the northern winter season the cold air controlled by the Arctic Oscillation and the Siberian High propagates southward along the eastern margin of the Tibetan Plateau and forms the strongest northerly dry and cold winter monsoon in the world, which plays an important role for the winter precipitation of the eastern Asian region (An, 2000; Wu and Wang, 2002). In general, however, the contribution of the winter precipitation to the whole year's precipitation amount is relatively small for the monsoonal East Asia. The meteorological data of the 13 counties of Xinjiang, China during 1951–1980 show that the ratio of mean precipitation amount in the autumn and winter seasons, including the snow amount, to the mean annual precipitation amount ranges from 20% to 50%, and the average value is only about 32% (Zhang and Deng, 1987). On the other hand, the relationship between the strength variations of the Asian summer monsoon and EAWM is still unclear, which suggests that the possible impacts of the Arctic Oscillation and the Siberian High on the Asian summer monsoons remain to be further studied.

3.4.5. Factors promoting an increase in the EASM strength during the YD

We have already shown evidence of the strengthened EASM and intensified westerlies during the YD and have used the dynamic process of convergence of the monsoon and westerlies in the atmosphere to explain the occurrence of rainfall in northern China during the period. Further clarifying the primary factor leading to an increase in the EASM strength during the YD would contribute to a better understanding of the global significance of the abnormal climate pattern of wet in the north and dry in the south. This factor should meet two conditions: it occurred in the YD period and it can lead to the inverse phase variation of the Asian monsoons on millennial timescales, i.e., the EASM strengthens while the ISM weakens.

In recent years, the impacts of the physical processes in the southern hemisphere on the ISM have attracted more and more attention. This is related to the nature of the ISM that is driven by cross-equatorial pressure gradient between the Indian low over the Asian continent and the Mascarene high in the southern Indian Ocean (Webster and Fasullo, 2003; An et al., 2011). As the Antarctic became warmer during the YD (Blunier and Brook, 2001; Koutavas et al., 2002), for instance, the Mascarene high would decrease and the Indian low would intensify, which would lead to a decrease in the cross-equatorial pressure gradient or a weakening of ISM. However, the impact of the southern hemisphere on the EASM remains unclear.

The El Niño-Southern Oscillation (ENSO) phenomenon in the tropical Pacific Ocean may be a candidate that may meet the two conditions mentioned above. Research on the cold tongue of the eastern equatorial Pacific has shown that the SST gradient in the equatorial Pacific decreased and that the Pacific was in an El Niño-like pattern during the YD and the OD periods (Koutavas et al., 2002). At the same time, investigations of the SST and salinity variability in the western tropical Pacific warm pool also published the same results (Stott et al., 2002). In particular, Stott et al. have suggested the following: “the shifts in the tropical Pacific ocean/atmosphere system are analogous to modern ENSO. El Niño conditions correlate with stadials at high latitudes, whereas La Niña conditions correlate with interstadials (Page 222 of Stott et al., 2002).”

Although the impact of paleo-ENSO on the monsoon during the YD remains unclear, research regarding the influence of modern ENSO on the Asian monsoon has been conducted over the past two decades. A statistical analysis of the relationship between the ISM rainfall and ENSO over the past 100 years suggested that ISM rainfall tends to weaken in an El Niño year and to strengthen in a La Niña year (Shukla and Paolina, 1983). This relationship may be strong enough to forecast incidences of ENSO (Webster et al., 1998). Later, a simulation study noted that severe droughts in India have always been accompanied by El Niño events, although El Niño events have not always produced severe droughts, which may depend on the tropical Pacific SST anomaly pattern associated with different ENSO events (Kumar et al., 2006). Another simulation study using a global coupled climate model (the Parallel Climate Model) also found that the precipitation variability in the Indian monsoon region is closely tied to a multidecadal pattern of SST anomalies in the Pacific Ocean. When the eastern Pacific SST warms, the Indian monsoon region experiences dry conditions, and vice versa (Meehl and Hu, 2006).

In the East Asian monsoon region, the modern EASM rainfall shows a significant spatial and temporal variation on interannual timescales, which has been attributed to the migration of a monsoonal rain belt and to the variation of monsoon intensity. In general, in April or May of every spring, an EASM rain belt is situated over the South China Sea region. In late May or early June, the rain belt moves to the southern region of the Yangtze River. Then, the rain belt will suddenly jump northward to the region between the Yangtze River and the Huaihe River on the Chinese mainland, Japan, and South Korea. This marks the beginning of the Meiyu season in China's Yangtze River-Huaihe River basin and of Japan's Baiu and South Korean's Changma seasons. In early or mid-July, the rain belt of the monsoon will again jump northward to a region in northern China, northeast China, and North Korea, indicating the

end of the Meiyu season in the Yangtze River-Huaihe River region and the beginning of the rainy season in northern regions of China. After the middle of August, the monsoonal rain belt generally moves quickly back to southern China. This phenomenon shows the so-called three settlements and two skip motions of a monsoonal rain belt over the Chinese mainland (Huang et al., 2008). Therefore, the rainfall distribution over the EASM region depends on the propagation speed of the monsoonal rain belt and on the length of time it remains over a given area. This situation often results in anomalous rainfall patterns on interannual timescales, with either floods in the north and drought in the south that usually reflect a stronger monsoon, or drought in the north and floods in the south on the Chinese mainland that usually indicate a weaker monsoon (Zhou and Yu, 2005). For example, during the period from 1951 to 1965, precipitation in northern China was much higher than the perennial mean value. From 1965 to 1976, precipitation in the Chinese mainland began to show oscillations. Starting around 1977, the rainfall decreased and continuous drought conditions have occurred in northern China (Huang et al., 2008). According to the rainfall data in recent years meteorologists tend to believe that the rainfall amounts in northern China may have again begun to increase, while precipitation in southern China may have started to decrease.

Previous studies have revealed that the EASM variation on interannual timescales is closely related to both the intensity and position of the western Pacific subtropical high (STH) and the thermal conditions of the equatorial Pacific (Tao and Chen, 1987). The results from numerical analysis and modeling have further suggested that the interannual variation of the STH reflects the variation in EASM intensity. When the SST variation in the equatorial east-middle Pacific takes on an El Niño-like pattern, the STH tends to strengthen. The STH over the western Pacific moves to the north, resulting in the northward migration of a precipitation belt toward China. This migration results in an increase in rainfall in northern China and, concurrently, less rainfall in the southern regions of China. Conversely, when the SST variation in the equatorial east-middle Pacific takes on a La Niña-like pattern, the STH tends to weaken and its location over the western Pacific moves to the south. This pattern generally results in the migration of the precipitation belt to the southern regions of China, with an increase in precipitation in the south but less rainfall in the north (Sun and Ying, 1999; Ying and Sun, 2000; Wu et al., 2003). The numerical analysis also demonstrated that when the equatorial east-middle Pacific is in a warm phase or in an El Niño-like pattern and the EASM strengthens, the ISM tends to weaken (Sun and Ying, 1999), which implies the occurrence of the inverse phase variation of the two Asian monsoons. This pattern coincides with the results from the ISM region mentioned previously.

In addition, to understand the phase response of the monsoonal circulation to insolation forcing at the Earth-orbital obliquity band (41 ka), the inverse phase variations between the ISM and EASM were recently simulated by a fully coupled global climate model (GCM) using a new phase mapping approach (Chen et al., 2011). In that study, the EASM characterized by precipitation in the northern Chinese continent (30–42°N, 105–140°E) and in the southern Chinese continent (20–30°N, 105–140°E) are called the NEASM and the SEASM, respectively. The simulations show that the ISM and the SEASM are in-phase and that the NEASM is out of phase with the ISM at the obliquity band (Chen et al., 2011). Another 46-ka transient accelerated simulation with the NCAR Community Climate System Model version 3 (CCSM3) shows that strengthened southeasterly wind anomalies appear over the central high latitudes of East Asia when the STH over the northwest Pacific (NWP) strengthens, transporting more moisture from the NWP to the EASM region, increasing precipitation in northern China, and decreasing precipitation in South China. Thus, the changes in the EASM precipitation forced by precessional variations exhibit a seesaw pattern between North and South China (Wang et al., 2012b). These results coincide with the aforementioned results that are the reported in Section 3.2, although their timescales are different.

In summary, the evidence from observations and simulations has shown that inverse phase variations between the ISM and EASM can occur on interannual and orbital timescales. However, additional simulations are required to further explore the potential dynamic relationship between the El Niño-like pattern, strengthened EASM, and weakened ISM during the YD cooling event on millennial timescales. If this dynamic relationship exists, it would highlight a unique scenario of global changes during the YD. At that time, accompanied by the occurrence of Melt Water Pulse IB and the cooling air temperature in the high northern latitudes (Fairbanks, 1989; Broecker, 2003) and by the El Niño-like activity in the equatorial Pacific (Koutavas et al., 2002; Stott et al., 2002), both the EASM and westerlies strengthened while the ISM weakened. Together these responses resulted in the abnormal climate pattern of wet in the north and dry in the south in East Asia.

It is worth emphasizing, however, that two different types of monsoon processes could cause this southern arid zone from southeastern China westward toward the remainder of southern Asia (Fig. 5). One process is a migration of the EASM rainfall belt to the north along with a strengthened EASM, which leads to less rainfall in southeastern China. In this case, the weakening of the EASM inferred simply from the arid climate in southeastern China is only an illusion. The increased aridness in southeastern China reflects only a false weakening of the EASM. The other monsoon process, as previous studies have indicated, is a real weakening of the ISM, which leads to little moisture being transported to the ISM region. In turn, this process leads to regional drought from the Tibetan Plateau to South Asia. Understanding the climate differences caused by the inverse variations of the two Asian monsoons is an important basis for global comparisons among paleoclimate records, research on climate dynamics, and investigating the relationship between climate change and ancient civilizations.

3.5. Response of the Asian summer monsoon to the forcing of GHGs and ENSO during the BA interstadial

During the BA warming period the Earth's climate system also experienced large changes: ice sheets decayed, resulting in a global mean sea level rise; terrestrial and marine ecosystems experienced large disturbances, resulting in a net release of the greenhouse gases CO_2 and CH_4 to the atmosphere; and changes in atmospheric and oceanic circulation affected the global distribution and fluxes of water and heat (Clark et al., 2012). In addition, it was during this period that the temperature pattern in the tropical Pacific showed a change from a decreasing gradient to an increasing gradient, indicating a transition from an El Niño-like pattern in the Last Glacial Maximum (LGM) to a La Niña-like pattern in the BA (Koutavas et al., 2002; Stott et al., 2002). Indeed, the Yuexi peat records the transition from a weak ISM in the OD to a strong ISM in BA (Fig. 4h, i) as a response to this changing SST gradient. However, the expected transition from a strong to a weak EASM does not occur, and the intensity of the EASM continues to increase during the BA period, as recorded in a variety of proxy indicators from the northern Chinese mainland and adjacent regions (Fig. 4a–g). This discrepancy possibly implies that for this transition period, the climate forcing factor was not limited to ENSO activity and that there may be other forcing mechanism.

When the BA warming event was recorded in the Greenland ice core (Stuiver et al., 1995), a clear cooling event, named as the Antarctic Cold Reversal (ACR), was recorded in the Antarctic ice core during the same period (Blunier and Brook, 2001). This seesaw effect of the climate system (Stocker, 1998) would increase the cross-equatorial pressure gradient between the Indian low and the Mascarene high and would lead to strengthening of the ISM. The impact of the seesaw effect on the EASM, however, remains to be elucidated.

The abruptly increasing concentration of CO_2 and CH_4 in the atmosphere, particularly the latter, at the transient interval from the LGM to BA has been considered as a main cause of the climate warming during the BA (Shakun and Carlson, 2010; Clark et al., 2012). The climate warming would have generated plenty of heat and moisture, which in turn would be favorable for increased rainfall in a widespread area covering the entire Asian monsoon region (Bengtsson, 2010). One supporting piece of evidence is that the maximum rainfall did not occur in the Bølling but in the Allerød period, regardless of the ISM or EASM regions (Fig. 4). It was only in the Allerød period, however, that the concentration of global atmospheric CH_4 reached its maximum (Grootes et al., 1993; Brook et al., 2000). It is noteworthy that in a comprehensive consideration to the effects of GHGs and ENSO, a recent modeling suggests a large increase in wetness over Central, East, and South Asia during the 21st century (Dai, 2013). If this hypothesis were correct, an increasing amount of rainfall in the entire Asian monsoon region would be expected in the future if the current climate continues to warm and the atmospheric concentrations of GHGs continue to rise.

4. Conclusions

The Yuexi peat cellulose $\delta^{13}C$ time series is a sensitive proxy record for the ISM. The record again confirms an important phenomenon in which the strength of the ISM abruptly decreases during the YD and OD stadial events and during a series of IRD cold events in the Holocene. The Yuexi peat also clearly records an increase in ISM strength during the BA interstadial, particularly in the Allerød warm period.

Comparisons between the Yuexi peat and other related proxy climate records show that during the YD, the two Asian monsoons showed inverse phase variations, with the ISM decreasing while the EASM increased, similar to the anti-phase variations in the IRD events of the Holocene.

Corresponding to the inverse phase variations during the YD, a wetter climate occurs in the northern Chinese mainland and a drier climate occurs in the south. It should be emphasized that the cause of this drier climate in southern China should be attributed to two different types of monsoon processes. One is a migration of the EASM rainfall belt to the north along with enhancement of the strength of the EASM, leading to less rainfall in southeastern China. Therefore, this weakening of the EASM inferred by the drier climate in southeastern China is only an illusion. The other monsoon process is a real weakening of the ISM, as indicated by the Yuexi peat $\delta^{13}C$ and the Dongge Cave stalagmite $\delta^{18}O$, leading to regional drought in southwestern China.

The abnormal climate pattern of wet in the north and dry in the south during the YD results from the combined effects of the strengthened EASM, intensified westerlies, and the weakened ISM, which could be attributed to the response to the abrupt cooling in the high northern latitudes and to the El Niño-like activity in the equatorial Pacific.

The wetter climate occurred in a widespread area covering the entire Asian monsoon region during the BA interstadial, which could be related to an increase in GHGs concentrations in the atmosphere and to the thermal condition in the equatorial Pacific. The impacts of the seesaw effect of the climate system on the two Asian monsoons remain to be clarified.

Acknowledgments

We sincerely thank J. Shulmeister and other anonymous referees for their thoughtful reviews and suggestions. This work was supported by the National Natural Science Foundation of China (grant Nos. 41173127, 41373134, and 40973089).

References

An, Z.S., 2000. The history and variability of the East Asian paleomonsoon climate. Quat. Sci. Rev. 19, 171–187.

An, Z.S., Clemens, S.C., Shen, J., Qiang, X.K., Jin, Z.D., Sun, Y.B., Prell, W.L., Luo, J.J., Wang, S.M., Xu, H., Cai, Y.J., Zhou, W.J., Liu, X.D., Liu, W.G., Shi, Z.G., Yan, L.B., Xiao, X.Y., Chang, H., Wu, F., Ai, L., Lu, F.Y., 2011. Glacial–interglacial Indian summer monsoon dynamics. Science 333, 719–723.

An, Z.S., Colman, S.M., Zhou, W.J., Li, X.Q., Brown, E.T., Jull, A.J.T., Cai, Y.J., Huang, Y.S., Lu, X.F., Chang, H., Song, Y.G., Sun, Y.B., Xu, H., Liu, W.G., Jin, Z.D., Liu, X.D., Cheng, P., Liu, Y., Ai, L., Li, X.Z., Liu, X.J., Yan, L.B., Shi, Z.G., Wang, X.L., Wu, F., Qiang, X.K., Dong, J.B., Lu, F.Y., Xu, X.W., 2012. Interplay between the Westerlies and Asian monsoon recorded in Lake Qinghai sediments since 32 ka. Sci. Rep. 2, 619 http://dx.doi.org/10.1038/srep00619.

An, Z.S., Porter, S.C., Zhou, W.J., Lu, Y.C., Donahue, D.J., Head, M.J., Wu, X.H., Ren, J.Z., Zheng, H.B., 1993. Episode of strengthened summer monsoon climate of Younger Dryas age on the loess plateau of central China. Quat. Res. 39, 45–54.

Bengtsson, L., 2010. The global atmospheric water cycle. Environ. Res. Lett. 5 http://dx.doi.org/10.1088/1748-9326/5/2/025002.

Blunier, T., Brook, E.J., 2001. Timing of millennial-scale climate change in Antarctica and Greenland during the last glacial period. Science 291, 109–112.

Blyakharchuk, T.A., Wright, H.E., Borodavko, P.S., van der Knaap, W.O., Ammann, B., 2007. Late Glacial and Holocene vegetational history of the Altai Mountains (southwestern Tuva Republic, Siberia). Palaeogeogr. Palaeoclimatol. Palaeoecol. 245, 518–534.

Bond, G., Showers, W., Cheseby, M., Lotti, R., Almasi, P., deMenocal, P., Priore, P., Cullen, H., Hajdas, I., Bonani, G., 1997. A pervasive millennial-scale cycle in North Atlantic Holocene and glacial climates. Science 278, 1257–1266.

Briggs, D.E.G., Evershed, R.P., Lockheart, M.J., 2000. The biomolecular paleontology of continental fossils. Paleobiology 26, 169–193.

Brook, E.J., Harder, S., Severinghaus, J., Steig, E.J., Sucher, C.M., 2000. On the origin and timing of rapid changes in atmospheric methane during the last glacial period. Glob. Biogeochem. Cycles 14, 559–572.

Broecker, W.S., 2003. Does the trigger for abrupt climate change reside in the ocean or in the atmosphere? Science 300, 1519–1522.

Cai, B.G., Edwards, L., Cheng, H., Tan, M., Wang, X., Liu, T.S., 2008. A dry episode during the Younger Dryas and centennial-scale weak monsoon events during the early Holocene: a high-resolution stalagmite record from southeast of the Loess Plateau, China. Geophys. Res. Lett. 35, L02705 http://dx.doi.org/10.1029/2007GL030986.

Chen, F.H., Bloemendal, J., Wang, J.M., Li, J.J., Oldfield, F., 1997. High-resolution multi-proxy climate records from Chinese loess: evidence for rapid climatic changes over the last 75 kyr. Palaeogeogr. Palaeoclimatol. Palaeoecol. 130, 323–335.

Chen, F.H., Yu, Z.C., Yang, M.L., Ito, E., Wang, S.M., Madsen, D.B., Huang, X.Z., Zhao, Y., Sato, T., Birks, H.J.B., Boomer, I., Chen, J.H., An, C.B., Wünnemann, B., 2008. Holocene moisture evolution in arid central Asia and its out-of-phase relationship with Asian monsoon history. Quat. Sci. Rev. 27, 351–364.

Chen, G.S., Liu, Z., Clemens, S.C., Prell, W.L., Liu, X.D., 2011. Modeling the time-dependent response of the Asian summer monsoon to obliquity forcing in a coupled GCM: a PHASEMAP sensitivity experiment. Clim. Dyn. 36, 695–710.

Clark, P.U., Shakun, J.D., Baker, P.A., Bartlein, P.J., Brewer, S., Brook, E., Carlson, A.E., Cheng, H., Kaufman, D.S., Liu, Z., Marchitto, T.M., Mix, A.C., Morrill, C., Otto-Bliesner, B.L., Pahnke, K., Russell, J.M., Whitlock, C., Adkins, J.F., Blois, J.L., Clark, J., Colman, S.M., Curry, W.B., Flower, B.P., He, F., Johnson, T.C., Lynch-Stieglitz, J., Markgraf, V., McManus, J., Mitrovica, J.X., Moreno, P.I., Williams, J.W., 2012. Global climate evolution during the last deglaciation. Proc. Natl. Acad. Sci. U. S. A. 109, E1134–E1142.

Colin, C., Siani, G., Sicre, M.-A., Liu, Z., 2010. Impact of the East Asian monsoon changes on the erosion of the Mekong River basin over the past 25000 yr. Mar. Geol. 271, 84–92.

Cook, C.G., Jones, R.T., Langdon, P.G., Leng, M.J., Zhang, E.N., 2011. New insights on Late Quaternary Asian palaeomonsoon variability and the timing of the Last Glacial Maximum in southwestern China. Quat. Sci. Rev. 30, 808–820.

Coplen, T.B., 1996. New guidelines for reporting stable hydrogen, carbon, and oxygen isotope-ratio data. Geochim. Cosmochim. Acta 60, 3359–3360.

Dai, A., 2013. Increasing drought under global warming in observations and models. Nat. Clim. Change 3, 52–58.

Dykoski, C.A., Edwards, R.L., Cheng, H., Yuan, D.X., Cai, Y.J., Zhang, M.L., Lin, Y.S., Qing, J.M., An, Z.S., Revenaugh, J., 2005. A high-resolution absolute-dated

Holocene and deglacial Asian monsoon record from Dongge Cave, China. Earth Planet. Sci. Lett. 233, 71–86.
Fairbanks, R.G., 1989. A 17,000-year glacio-eustatic sea level record: influence of glacial melting rates on the Younger Dryas event and deep-ocean circulation. Nature 342, 637–642.
Fleitmann, D., Burns, S.J., Mudelsee, M., Neff, U., Kramers, J., Mangini, A., Matter, A., 2003. Holocene forcing of the Indian monsoon recorded in a stalagmite from Southern Oman. Science 300, 1737–1739.
Fleitmann, D., Burns, S.J., Mangini, A., Mudelsee, M., Kramers, J., Villa, I., Neff, U., Al-Subbary, A.A., Buettner, A., Hippler, D., Matter, A., 2007. Holocene ITCZ and Indian monsoon dynamics recorded in stalagmites from Oman and Yemen (Socotra). Quat. Sci. Rev. 26, 170–188.
Francey, R.J., Farquhar, G.D., 1982. An explanation of $^{13}C/^{12}C$ variations in tree rings. Nature 297, 28–31.
Gao, Y.X., Xu, S.Y., Guo, Q.Y., 1962. Monsoon region and regional climate in China. In: Gao, Y.X., Xu, S.Y. (Eds.), Some Problems of East Asian Monsoon. Science Press, Beijing, pp. 49–63 (in Chinese).
Gasse, F., Arnold, M., Fontes, J.C., Fort, M., Gibert, E., Huc, A., Li, B.Y., Li, Y.F., Liu, Q., Mélières, F., Campo, E.V., Wang, F.B., Zhang, Q.S., 1991. A 13,000-year climate record from western Tibet. Nature 353, 742–745.
Green, J.W., 1963. Wood cellulose. In: Whistler, R.L. (Ed.), Methods in Carbohydrate Chemistry, vol. 3. Academic Press, New York, pp. 9–22.
Grootes, P.M., Stuiver, M., White, J.W.C., Johnsen, S., Jouzel, J., 1993. Comparison of oxygen isotope record from the GISP2 and GRIP Greenland ice cores. Nature 366, 552–554.
Gupta, A.K., Anderson, D.M., Overpeck, J.T., 2003. Abrupt changes in the Asian southwest monsoon during the Holocene and their links to the North Atlantic Ocean. Nature 421, 354–357.
Hong, B., Hong, Y.T., Lin, Q.H., Shibata, Y., Uchida, M., Zhu, Y.X., Leng, X.T., Wang, Y., Cai, C.C., 2010. Anti-phase oscillation of Asian monsoons during the Younger Dryas period: evidence from peat cellulose $\delta^{13}C$ of Hani, Northeast China. Palaeogeogr. Palaeoclimatol. Palaeoecol. 297, 214–222.
Hong, B., Hong, Y.T., Lin, Q.H., Zhu, Y.X., Leng, X.T., Wang, Y., Cai, C.C., 2011. Reply to comment on "Anti-phase oscillation of Asian monsoons during the Younger Dryas period: evidence from peat cellulose $\delta^{13}C$ of Hani, Northeast China" by B. Hong, Y.T. Hong, Q.H. Lin, Y. Shibata, M. Uchida, Y.X. Zhu, X.T. Leng, Y.Wang and C.C. Cai [Palaeogeography, Palaeoclimatology, Palaeoecology 297 (2010) 214–222]. Palaeogeogr. Palaeoclimatol. Palaeoecol. 306, 98–101.
Hong, Y.T., Hong, B., Lin, Q.H., Shibata, Y., Hirota, M., Zhu, Y.X., Leng, X.T., Wang, Y., Wang, H., Yi, L., 2005. Inverse phase oscillations between the East Asian and Indian Ocean summer monsoons during the last 12000 years and paleo-El Niño. Earth Planet. Sci. Lett. 231, 337–346.
Hong, Y.T., Hong, B., Lin, Q.H., Zhu, Y.X., Shibata, Y., Hirota, M., Uchida, M., Leng, X.T., Jiang, H.B., Xu, H., Wang, H., Yi, L., 2003. Correlation between Indian Ocean summer monsoon and North Atlantic climate during the Holocene. Earth Planet. Sci. Lett. 211, 371–380.
Hong, Y.T., Jiang, H.B., Liu, T.S., Zhou, L.P., Beer, J., Li, H.D., Leng, X.T., Hong, B., Qin, X.G., 2000. Response of climate to solar forcing recorded in a 6000-year $\delta^{18}O$ time series of Chinese peat cellulose. Holocene 10, 1–7.
Hong, Y.T., Wang, Z.G., Jiang, H.B., Lin, Q.H., Hong, B., Zhu, Y.X., Wang, Y., Xu, L.S., Leng, X.T., Li, H.D., 2001. A 6000-year record of changes in drought and precipitation in northeastern China based on a $\delta^{13}C$ time series from peat cellulose. Earth Planet. Sci. Lett. 185, 111–119.
Huang, R.H., Gu, L., Chen, J.L., Huang, G., 2008. Recent progress in studies of the temporal–spatial variations of the East Asian monsoon system and their impacts on climate anomalies in China. Chin. J. Atmos. Sci. 32, 691–719 (in Chinese with English summary).
Huang, Y., Jiang, H., Sarnthein, M., Knudsen, K.L., Li, D.L., 2009. Diatom response to changes in palaeoenvironments of the northern South China Sea during the last 15000 years. Mar. Micropaleontol. 72, 99–109.
Jarvis, D.I., 1993. Pollen evidence of Changing Holocene monsoon climate in Sichuan province, China. Quat. Res. 39, 325–337.
Ji, J.F., Shen, J., Balsam, W., Chen, J., Liu, L.W., Liu, X.Q., 2005. Asian monsoon oscillations in the northeastern Qinghai-Tibet Plateau since the late glacial as interpreted from visible reflectance of Qinghai Lake sediments. Earth Planet. Sci. Lett. 233, 61–70.
Kelts, K., Chen, K.Z., Lister, G., Yu, J.Q., Gao, Z.H., Nissen, F., Bonani, G., 1989. Geological fingerprints of climate history: a cooperative study of Qinghai Lake, China. Eclogae Geol. Helvet. 82, 167–182.
Koutavas, A., Lynch-Stieglitz, J., Marchitto, T.M., Sachs, J.P., 2002. El Niño-like pattern in Ice Age tropical Pacific sea surface temperature. Science 297, 226–230.
Kumar, K.K., Rajagopalan, B., Hoerling, M., Bates, G., Cane, M., 2006. Unraveling the mystery of Indian monsoon failure during El Niño. Science 314, 115–119.
Lee, S.H., Lee, Y.I., Yoon, H.I., Yoo, K.C., 2008. East Asian monsoon variation and climate changes in Jeju Island, Korea, during the latest Pleistocene to early Holocene. Quat. Res. 70, 265–274.
Li, X.Q., Zhao, K.L., Dodson, J., Zhou, X.Y., 2011. Moisture dynamics in central Asia for the last 15 kyr: new evidence from Yili Valley, Xinjiang, NW China. Quat. Sci. Rev. 30, 3457–3466.
Liu, X.Q., Dong, H.L., Rech, J.A., Matsumoto, R., Bo, Y., Wang, Y.B., 2008. Evolution of Chaka Salt Lake in NW China in response to climatic change during the latest Pleistocene–Holocene. Quat. Sci. Rev. 27, 867–879.
Ma, Z.B., Cheng, H., Tan, M., Edwards, R.L., Li, H.C., You, C.F., Duan, W.H., Wang, X., Kelly, M.J., 2012. Timing and structure of the Younger Dryas event in northern China. Quat. Sci. Rev. 41, 83–93.
Meehl, G.A., Hu, A., 2006. Megadroughts in the Indian monsoon region and southwest North America and a mechanism for associated multidecadal pacific sea temperature anomalies. J. Clim. 19, 1605–1623.
Morrill, C., Overpeck, J.T., Cole, J.E., 2003. A synthesis of abrupt changes in the Asian summer monsoon since the last deglaciation. Holocene 13, 465–476.
Rhodes, T.E., Gasse, F., Lin, R.F., Fontes, J.C., Wei, K.Q., Bertrand, P., Gibert, E., Melieres, F., Tucholka, P., Wang, Z.X., Cheng, Z.Y., 1996. A Late Pleistocene–Holocene lacustrine record from Lake Manas, Zunggar (Northern Xinjiang, Western China). Palaeogeogr. Palaeoclimatol. Palaeoecol. 120, 105–121.
Rudaya, N., Tarasov, P., Dorofeyuk, N., Solovieva, N., Kalugin, I., Andreev, A., Daryin, A., Diekmann, B., Riedel, F., Tserendash, N., Wagner, M., 2009. Holocene environments and climate in the Mongolian Altai reconstructed from the Hoton-Nur pollen and diatom records: a step towards better understanding climate dynamics in Central Asia. Quat. Sci. Rev. 28, 540–554.
Schettler, G., Liu, Q., Mingram, J., Stebich, M., Dulski, P., 2006. East-Asian monsoon variability between 15000 and 2000 cal. yr BP recorded in varved sediments of Lake Sihailongwan (northeastern China, Long Gang volcanic filed). Holocene 16, 1043–1057.
Schleser, G.H., 1995. Parameters determining carbon isotope ratios in plants. In: Frenzel, B., Stauffer, B., Weiss, M.M. (Eds.), Paläoklimaforschung 15 Strasbourg, France, pp. 71–96.
Seki, O., Meyers, P.A., Kawamura, K., Zheng, Y., Zhou, W., 2009. Hydrogen isotopic ratios of plant wax *n*-alkanes in a peat bog deposited in northeast China during the last 16 kyr. Org. Geochem. 40, 671–677.
Shakun, J.D., Carlson, A.E., 2010. A global perspective on Last Glacial Maximum to Holocene climate change. Quat. Sci. Rev. 29, 1801–1816.
Shinozaki, T., Uchida, M., Minoura, K., Kondo, M., Rella, S.F., Shibata, Y., 2011. Synchronicity of the East Asian summer monsoon variability and northern Hemisphere climate change since the last deglaciation. Clim. Past Discuss. 7, 2159–2192.
Shukla, J., Paolina, D., 1983. The Southern oscillation and long range forecasting of the summer monsoon rainfall over India. Mon. Weather Rev. 111, 1830–1837.
Sofer, Z., 1980. Preparation of carbon dioxide for stable carbon isotope analysis of petroleum fractions. Anal. Chem. 52, 1389–1391.
Stebich, M., Mingram, J., Han, J.T., Liu, J.Q., 2009. Late Pleistocene spread of (cool-) temperate forests in northeast China and climate changes synchronous with the North Atlantic region. Global Planet. Change 65, 56–70.
Stocker, T.F., 1998. The Seesaw effect. Science 282 (5386), 61–62.
Stott, L., Poulsen, C., Lund, S., Thunell, R., 2002. Super ENSO and global climate oscillations at millennial time. Science 297, 222–226.
Stuiver, M., Grootes, P.M., Braziunas, T.F., 1995. The GISP2 $\delta^{18}O$ climate record of the past 16500 years and the role of the sun, ocean, and volcanoes. Quat. Res. 44, 341–354.
Stuiver, M., Reimer, P.J., Bard, E., Beck, J.W., Burr, G.S., Hughen, K.A., Kromer, B., McCormac, F.G., Plicht, J.V.D., Spurk, M., 1998. Radiocarbon calibration program rev 4.3. Radiocarbon 40, 1041–1083.
Sun, S.Q., Ying, M., 1999. Subtropical high anomalies over the Western Pacific and its relations to the Asian monsoon and SST anomaly. Adv. Atmos. Sci. 16, 559–568.
Tao, S., Chen, L., 1987. A review of recent research on the East Asian summer monsoon in China. In: Chang, C.P., Krishnamurti, T.N. (Eds.), Monsoon Meteorology. Oxford University Press, Oxford, pp. 60–92.
Tarasov, P., Dorofeyuk, N., Metel'tseva, E., 2000. Holocene vegetation and climate changes in Hoton-Nur basin, northwest Mongonia. Boreas 29, 117–126.
Tarasov, P., Williams, J.W., Andreev, A., Nakagawa, T., Bezrukova, E., Herzschuh, U., Igarashi, Y., Müller, S., Werner, K., Zheng, Z., 2007. Satellite- and pollen-based quantitative woody cover reconstructions for northern Asia: verification and application to late-Quaternary pollen data. Earth Planet. Sci. Lett. 264, 284–298.
Tiwari, M., Singh, A.K., Ramesh, R., 2011. High-resolution monsoon records since Last Glacial Maximum: a comparison of marine and terrestrial paleoarchives from South Asia. J. Geol. Res. 2011, 1–12.
Uchida, M., et al., 2008. Radiocarbon-based carbon source quantification of anomalous isotopic foraminifera in last glacial sediments in the western North Pacific. Geochem. Geophys. Geosyst. 9, Q04N14 http://dx.doi.org/10.1029/2006GC001558.
Wang, B., Clemens, S.C., Liu, P., 2003. Contrasting the Indian and East Asian monsoons: implications on geologic timescales. Mar. Geol. 201, 5–21.
Wang, H., Hong, Y.T., Lin, Q.H., Hong, B., Zhu, Y.X., Wang, Y., Xu, H., 2010. Response of humification degree to monsoon climate during the Holocene from the Hongyuan peat bog, eastern Tibetan Plateau. Palaeogeogr. Palaeoclimatol. Palaeoecol. 286, 171–177.
Wang, H.J., Chen, H.P., 2012. Climate control for southeastern China moisture and precipitation: Indian or East Asian monsoon? J. Geophys. Res. 117, D12109 http://dx.doi.org/10.1029/2012JD017734.
Wang, X., Ding, Z.L., Peng, P.A., 2012a. Changes in fire regimes on the Chinese Loess Plateau since the last glacial maximum and implications for linkages to paleoclimate and past human activity. Palaeogeogr. Palaeoclimatol. Palaeoecol. 315–316, 61–74.
Wang, X.F., Auler, A.S., Edwards, R.L., Cheng, H., Ito, E., Solheid, M., 2006. Interhemispheric anti-phasing of rainfall during the last glacial period. Quat. Sci. Rev. 25, 3391–3403.
Wang, Y., Cheng, H., Edwards, R.L., An, Z.S., Wu, J.Y., Shen, C.C., Dorale, J.A., 2001. A high-resolute absolute-dated Late Pleistocene monsoon record from Hulu Cave, China. Science 294, 2345–2348.

Wang, Y., Cheng, H., Edwards, R.L., He, Y., Kong, X., An, Z., Wu, J., Kelly, M.J., Dykoski, C.A., Li, X., 2005. The Holocene Asian monsoon: links to solar changes and North Atlantic climate. Science 308, 854–857.

Wang, Y., Jian, Z.M., Zhao, P., 2012b. Extratropical modulation on Asian summer monsoon at precessional bands. Geophys. Res. Lett. 39, L14803, http://dx.doi.org/10.1029/2012GL052553.

Wang, Y.J., Cheng, H., Edwards, R.L., Kong, X., Shao, X., Chen, S., Wu, J., Jiang, X., Wang, X., An, Z., 2008. Millennial- and orbital-scale changes in the East Asian monsoon over the past 224000 years. Nature 451, 1090–1093.

Wanner, H., Solomina, O., Grosjean, M., Ritz, S.P., Jetel, M., 2011. Structure and origin of Holocene cold events. Quat. Sci. Rev. 30, 3109–3123.

Webster, P.J., Fasullo, J., 2003. Dynamic theory of monsoons. In: Holton, J., Curry, J.A. (Eds.), Encyclopedia of Atmospheric Sciences. Academic Press, London, pp. 1370–1386.

Webster, P.J., Magana, V.O., Palmer, T.N., Shukla, J., Tomas, R.A., Yanai, M., Yasunari, T., 1998. Monsoons: processes, predictability, and the prospects for prediction. J. Geophys. Res. 103, 14451–14510.

Winkler, M.G., Wang, P.K., 1993. The Late Quaternary vegetation and climate of China. In: Wright, H.E. (Ed.), Global Climates Since the Last Glacial Maximum. University of Minnesota Press, Minneapolis, pp. 221–261.

Wu, B., Wang, J., 2002. Winter Arctic oscillation, Siberian high and East Asian winter monsoon. Geophys. Res. Lett. 29 http://dx.doi.org/10.1029/2002GL015373.

Wu, G.X., Chou, J.F., Liu, Y.M., Zhang, Q.Y., Sun, S.Q., 2003. Review and prospect of the study on the subtropical anticyclone. Chin. J. Atmos. Sci. 27, 503–517 (in Chinese with English summary).

Yang, X., Scuderi, L., Paillou, P., Liu, Z., Li, H., Ren, X., 2011. Quaternary environmental changes in the drylands of China – a critical review. Quat. Sci. Rev. 30, 3219–3233.

Yang, X., Wang, X., Liu, Z., Li, H., Ren, X., Zhang, D., Ma, Z., Rioual, P., Jin, X., Scuderi, L., 2013. Initiation and variation of the dune fields in semi-arid northern China – with a special reference to the Hunshandake Sandy Land, Inner Mongolia. Quat. Sci. Rev. 78, 369–380.

Ying, M., Sun, S.Q., 2000. A study on the response of subtropical high over the western Pacific on the SST anomaly. Chin. J. Atmos. Sci. 24, 193–206 (in Chinese with English summary).

Zhang, J.B., Deng, Z.F., 1987. An Introduction to Precipitation in the Xinjiang Autonomous Region. Meteorological Press, Beijing, pp. 132–156.

Zhong, W., 1998. The younger Dryas cooling event reflected by carbonate isotopic data from Bosten Lake sediment during late deglaciation. Mar. Geol. Quat. Geol. 18, 87–94.

Zhong, W., Xue, J.B., Cao, J.X., Zheng, Y.M., Ma, Q.H., Ouyang, J., Cai, Y., Zeng, Z.G., Liu, W., 2010. Bulk organic carbon isotopic record of lacustrine sediments in Dahu Swamp, eastern Nanling Mountains in South China: Implication for catchment environmental and climatic changes in the last 16 000 years. J. Asian Earth Sci. 38, 162–169.

Zhou, T.J., Yu, R.C., 2005. Atmospheric water vapor transport associated with typical anomalous summer rainfall patterns in China. J. Geophys. Res. 110, D08104 http://dx.doi.org/10.1029/2004JD005413.

Zhou, W., Zheng, Y., Meyers, P.A., Timothy Jull, A.J., Xie, S., 2010. Postglacial climate-change record in biomarker lipid compositions of the Hani peat sequence, Northeastern China. Earth Planet. Sci. Lett. 294, 37–46.

Zhou, W.J., Donahue, D.J., Porter, S.C., Jull, A.J.T., Li, X.Q., Stuiver, M., An, Z.S., Matsumoto, E., Dong, G.R., 1996. Variability of monsoon climate in East Asia at the end of the last glaciation. Quat. Res. 46, 219–229.

Zhou, W.J., Head, J.M., An, Z.S., Deckker, D.D., Liu, Z.L., Liu, X.D., Lu, X.F., Donahue, D., Jull, T.A.J., Beck, J.W., 2001. Terrestrial evidence for a spatial structure of tropical-polar interconnections during the Younger Dryas episode. Earth Planet. Sci. Lett. 191, 231–239.

Zhou, W.J., Yu, X.F., Jull, A.J.T., Burr, G., Xiao, J.Y., Lu, X.F., Xiao, F., 2004. High-resolution evidence from southern China of an early Holocene optimum and a mid-Holocene dry event during the past 18000 years. Quat. Res. 62, 39–48.

Zhu, C., Ma, C., Yu, S.Y., Tang, L., Zhang, W., Lu, X., 2009. A detailed pollen record of vegetation and climate changes in Central China during the past 16000 years. Boreas 39, 69–76.